Virus Research 251 (2018) 68–77

Contents lists available at ScienceDirect

Virus Research

journal homepage: www.elsevier.com/locate/virusres

Neutrophil extracellular traps possess anti-human respiratory syncytial virus activity: Possible interaction with the viral F protein

Priscila Silva Sampaio Souza[a,*], Lia Vezenfard Barbosa[a], Larissa Figueiredo Alves Diniz[a], Gabriel Soares da Silva[a], Bruno Rafael Pereira Lopes[a], Pedro Miyadaira Ribeiro Souza[a], Gabriela Campos de Araujo[b,c], Diogo Pessoa[a], Juliana de Oliveira[a], Fátima Pereira Souza[b,c], Karina Alves Toledo[a]

[a] Department of Biological Sciences, Universidade Estadual Paulista – UNESP (FCLAssis), Brazil
[b] Department of Physics, Universidade Estadual Paulista – UNESP (IBILCE, São José do Rio Preto), Brazil
[c] Centro Multiusuário de Inovação Biomolecular (CMIB), Universidade Estadual Paulista – UNESP (IBILCE, São José do Rio Preto), Brazil

ARTICLE INFO

Keywords:
Neutrophil extracellular traps
Respiratory syncytial virus
Molecular docking

ABSTRACT

Human respiratory syncytial virus (hRSV) is one of the main etiological agents of diseases of the lower respiratory tract, and is often responsible for the hospitalization of children and the elderly. To date, treatments are only palliative and there is no vaccine available. The airways of patients infected with hRSV exhibit intense neutrophil infiltration, which is responsible for the release of neutrophil extracellular traps (NETs). These are extracellular structures consisting of DNA associated with intracellular proteins, and are efficient in capturing and eliminating various microorganisms, including some viruses. hRSV induces the release of NETs into the lung tissue of infected individuals; however, the pathophysiological consequences of this event have not been elucidated. The objective of this study was to utilize *in vitro* and *in silico* assays to investigate the impact of NETs on hRSV infection. NETs, generated by neutrophils stimulated with phorbol myristate acetate (PMA), displayed long fragments of DNA and an electrophoretic profile suggestive of the presence of proteins that are classically associated with these structures (elastase, cathepsin G, myeloperoxidase, and histones). The presence of NETs (> 2 μg/ml) in HEp-2 cell culture medium resulted in cellular cytotoxicity of less than 50%. Pre-incubation (1 h) of viral particles (multiplicity of infection (MOI) values of 0.1, 0.5, and 1.0) with NETs (2–32 μg/ml) resulted in cellular protection from virus-induced death of HEp-2 cells. Concurrently, there was a reduction in the formation of syncytia, which is related to decreased viral spread in infected tissue. Results from western blotting and molecular docking, suggest interactions between F protein of the hRSV viral envelope and BPI (bactericidal permeability-increasing protein), a microbicidal member of NETs. Interactions occurred at sites important for the neutralization and coordination of the hRSV infection/replication process. Our results showed that the presence of NETs decreases hRSV-induced cellular damage, possibly by directly affecting viral particle capture and/or interfering with the fusion activity of the F protein. These findings broaden the understanding of the role of NETs during hRSV infection.

1. Introduction

Human respiratory syncytial virus (hRSV) is one of the major etiologic agents of lower respiratory tract infections in neonates, children, and the elderly, and might cause bronchiolitis, bronchitis, pneumonia, and chronic obstructive pulmonary infections (Hall et al., 1991). Among the currently available prevention measures is the administration of the Palivizumab antibody. However, the cost of administering this drug is very high and has only been used for the immunization of high-risk children (Huang et al., 2010).

In vitro airway epithelial cells infected with hRSV produce proinflammatory cytokines and chemokines that promote the activation and recruitment of immune system cells, resulting in increased neutrophil transmigration to the site (Rzepka et al., 2012). Neutrophils can be found in the airways of pulmonary disease patients infected with hRSV. Due to intense viral replication and leukocyte influx, the airways can

* Corresponding author at: Av. Dom Antônio, 2100, Parque Universitário, CEP 19806-900, Assis/SP, Brazil.
E-mail addresses: priscilasampaiosouza@gmail.com (P.S.S. Souza), lia.vezenfard@gmail.com (L.V. Barbosa), laridiniz9@gmail.com (L.F.A. Diniz), gaabrielsoares10@gmail.com (G.S. da Silva), brunorpl@hotmail.com (B.R.P. Lopes), pmiyadaira@outlook.com (P.M.R. Souza), bicamposaraujo@hotmail.com (G.C. de Araujo), diogo.pessoa@gmail.com (D. Pessoa), juliana@assis.unesp.br (J. de Oliveira), fatyssouza@gmail.com (F.P. Souza), karinafcla@gmail.com (K.A. Toledo).

https://doi.org/10.1016/j.virusres.2018.04.001
Received 26 June 2017; Received in revised form 2 November 2017; Accepted 1 April 2018
Available online 03 April 2018
0168-1702/ © 2018 Elsevier B.V. All rights reserved.

become blocked by excessive mucus production, edema, and cellular debris (Cortjens et al., 2016) worsening the patient's clinical status.

Neutrophils present at the site of infection release Neutrophil extracellular traps (NETs), which consist of DNA associated with intracellular proteins (granular, nuclear and cytoplasmic) such as elastase, histones, and myeloperoxidase. NETs have microbicidal action, specifically in relation to the capture and/or death of several pathogens including some viruses (Brinkmann et al., 2004; Jenne et al., 2013; Saitoh et al., 2012). Although the microbicidal action of NETs has been described for several pathogens, its beneficial role has been questioned with regard to several infectious and non-infectious human diseases. The excessive presence of NETs can cause tissue damage and accelerate the progression of some diseases including lung diseases (Porto and Stain, 2016).

The role of neutrophils in hRSV infections has not been elucidated. The airways of patients infected with hRSV accumulate mucus that is rich in DNA (Cortjens et al., 2016). It has been shown that the hRSV F protein can induce the release of NETs (Funchal et al., 2015). The F protein mediates viral envelope fusion to the cytoplasmic membrane, allowing for infection and fusion of infected cells with adjacent cells; this leads to the formation of syncytial, multinucleated giant cells, a cytopathic characteristic of hRSV infection (Collins et al., 2001).

The aim of the present study was to evaluate the role of NETs during *in vitro* hRSV infection. Western blotting and i*n silico* assays were performed to analyze possible interactions between NET components and the virus. This study helps to understand the role of NETs during viral infection and its relationship to hRSV and may contribute to future studies for the development of new treatments and strategies to combat hRSV, helping to reduce infections and control the disease.

2. Materials and methods

2.1. Cell culture

HEp-2 cells (oropharyngeal carcinoma, permissive for infection and replication of the hRSV virus) (Gupta et al., 1996), obtained from the Cell Bank of Rio de Janeiro (BCRJ), were cultured in 75 cm^2 culture bottles (Corning Glass Works, New York, NY, USA) incubated in a humidified incubator (37 °C, 5% CO_2) and DMEM F12 culture medium, (Sigma-Aldrich, Saint Louis, MO, USA) supplemented with 10% fetal bovine serum (SFB - Cultilab, Campinas, SP, Brazil) plus antibiotics and antimycotics (Gibco, Life Technologies, Gaithersburg, MD, USA).

2.2. Viral stock

Long strain hRSV virus, provided by Prof. Dr. Eurico de Arruda Neto (Free Professor of Virology, Medical School of Ribeirão Preto - USP), was used to inoculate HEp-2 cell cultures. Viral stocks were prepared in incomplete DMEM F12 (not containing added FBS) culture medium. After collecting the viral stock, the aliquots were frozen in DMEM F12 plus 10% trehalose and maintained at −80 °C until use (Gupta et al., 1996). The viral titer was established by the lysis plaque formation assay (Mckimm-Breschkin, 2004) and confirmed by the TCDI50 assay (Rasmussen et al., 2011).

2.3. Purification and stimulation of human neutrophils to generate NETs

Human neutrophils were isolated and stimulated according to the methodology described by Brinkmann et al. (2010), with modifications (Najmeh et al., 2015; Saffarzadeh et al., 2012). Peripheral blood from healthy volunteers was collected in the presence of sodium heparin and separated using Histopaque 1077 and 1119 (Sigma). The cell pellet was resuspended in DMEM F12 without FBS and overall counts were determined using a Neubauer's chamber (Neubauer Improved Bright-Line, Loptik Labor, Germany). Neutrophils were then stimulated by phorbol 12-myristate 13-acetate (PMA – Sigma) (50 nM) diluted in DMEM F12 without FBS. The absence of FBS is necessary due to the presence of DNAse, which could degrade the NETs (Von Köckritz-Blickwede et al., 2009). After incubation in a humidified incubator (3 h, 37 °C, 5% CO_2) the supernatant was discarded and the NETs were collected and incubated in a water bath at 40 °C for 24 h. The samples were aliquoted and stored at −25 °C. To quantify the DNA present in the samples, a Qubit 2.0 fluorimeter (Invitrogen Inc., Grand Island, NY, USA) was used with the PicoGreen® dsDNA Assay Kit (Invitrogen).

2.4. Visualization of NETs by fluorescence microscopy

Isolated neutrophils were added to a 24-well plate (2×10^5/well) containing coverslips treated with 0.01% poly-L-lysine (Sigma). Cells were stimulated with PMA (50 nM) for 3 h in a humidified incubator (37 °C, 5% CO_2). Unstimulated cells were used as a negative control for NET production. The coverslips were mounted using ProLong Gold containing DAPI (Invitrogen). Twenty-four hours later, the samples were imaged using a Nikon Eclipse Ti fluorescence inverted microscope coupled with a Nikon Sight digital camera.

2.5. Polyacrylamide gel electrophoresis

For analysis of the protein electrophoretic profile, NET aliquots (0.8–3.2 µg), diluted in Laemmli sample buffer (Sigma), were applied to 12% and 20% polyacrylamide gels, prepared according to the protocol of Green and Sambrook (2012). Precision Plus Protein Dual Color Standards (Bio-Rad Laboratories, Inc, 205 CA, USA) were used as the molecular weight marker. Subsequently, gels were stained with silver nitrate (Chevallet et al., 2006).

2.6. Agarose gel electrophoresis

For analysis of the DNA electrophoretic profile, NET aliquots (1 µg) were centrifuged at 10,200 xg for 10 min and subjected to 1.5% agarose gel electrophoresis. A 1-kb DNA ladder was used as the molecular weight standard (Kasvi, Curitiba, PR, Brazil). The gel was stained with GelRed (1:10,000) (Biotium, Hayward, CA, USA) and the images were visualized and captured using a photodocumentator ultraviolet transilluminator.

2.7. Evaluation of myeloperoxidase

In a 96-well plate, 50 µl/well of NETs (27 µg/ml) that had been incubated in a water bath for 24 h at 40 °C were added in triplicate. NETs not subjected to incubation, and referred to as fresh NETs, were also tested. Cell-free culture medium was used as the negative control for the reaction. Each well received 100 µl of 3′,5,5′-tetramethylbenzidine substrate (TMB, Wiener lab, Rosário, SF, Argentina). After 1 h of incubation (37 °C, 5% CO_2), the reaction was stopped with 1 N sulfuric acid. The absorbance of the solution was measured using a spectrophotometric apparatus (Multiskan™ FC Microplate Photometer) at 405 nm. The absorbance values were converted to a percentage of myeloperoxidase activity, assuming 100% activity for the absorbance values obtained using the fresh NET solution. Fresh NETs were collected immediately after a 3-h stimulation with PMA and incubated with 500 mU/ml micrococcal nuclease (Worthington Biochemical, Lakewood, NJ, USA) for 10 min at 37 °C. Fresh NETs were quantified after the addition of EDTA (5 mM) so that the digestion would be complete (Sousa-Rocha et al., 2015). NET samples incubated in a water bath for 24 h at 37 °C were included in the assay.

2.8. Determination of cellular cytotoxicity

HEp-2 cells grown in DMEM F12 culture medium plus 10% FBS were plated in a 96-well plate and incubated for 24 h, to obtain a confluency ≥80%. The culture medium was replaced with FBS-free

DMEM F12 containing different concentrations of NETs (0–67 μg/ml). The culture was maintained for 4 d in a humidified incubator (37 °C, 5% CO_2). HEp-2 cell viability was evaluated on the fourth day by performing a colorimetric assay using MTT salts [1-(4,5-Dimethylthiazol-2-yl)-3,5-diphenylformazan, thiazolyl blue formazan], following the manufacturer's recommendations (Sigma). The absorbance of the solution (560 nm) was obtained using a spectrophotometric apparatus (Multiskan™ FC Microplate Photometer) and the values were converted to the percentage of cells. Absorbance values were converted to percent viability assuming the cell culture control (cultured in the absence of NETs) to be 100% viability.

2.9. In vitro hRSV infection

HEp-2 cells were plated in 96-well plates (5×10^4/well) and maintained for 24 h in DMEM F12 culture medium supplemented with 10% FBS. The assay was performed as described by Petricevich and Mendonca (2003), with some modifications. hRSV suspensions (MOI of 0.1, 0.5, and 1 were incubated (1 h, 4 °C) in the presence of different concentrations of NETs (0–64 μg/ml). Subsequently, the culture medium from each well was replaced with NET-treated or untreated viral aliquots for further incubation (2 h, 37 °C). The viral inoculum was then discarded and wells were incubated for 4 d in a humidified incubator (37 °C and 5% CO_2) in the presence of serum free DMEM F12. Cell viability was assessed on the fourth day by performing colorimetric assays using MTT salts (as described previously), and absorbance was measured using a spectrophotometric apparatus at 560 nm. The assays included untreated and uninfected control groups (cell control) and an additional group of untreated and virus-infected cells (viral control). Absorbance values were converted into percent viable cells assuming the cell control to be 100% viability. The percent protection obtained using each treatment was calculated as follows:

$$Cellular\ Protection = \frac{OD_{TS} * 100}{OD_{CC100}} \quad (1)$$

Where:

OD is the optical density after reading the absorbance of the MTT salts at 560 nm;

OD_{TS} is the optical density obtained for each of the test samples − OD_{VC} (optical density of viral control), and

OD_{CC100} is $OD_{CC} - DO_{VC}$ (optical density of the control cell − optical density of viral control).

2.10. Statistical analysis

The experimental data were processed using Microsoft Excel® and GraphPad Prism® 6 and were evaluated by analysis of variance (one-way ANOVA), followed by the Bonferroni test. A level of significance of $p \leq 0.05$ was used. The number of replicates for each experiment is indicated in each respective figure.

2.11. Western blotting

Total NET solution was quantified using a bicinchoninic acid protein assay kit (Pierce, Biotechnology, Rockford, IL, USA). Next, 30 μg total protein was diluted in sample buffer [62.5 M Tris, pH 6.8, 2% SDS (w/v), 5% glycerol (v/v), 0.01% bromophenol blue]. Samples were resolved in 10% polyacrylamide gels and transferred onto nitrocellulose membranes (Amersham Biosciences, Amersham, UK). After blocking in 5% non-fat dry milk, the membranes were incubated with RSV for 16 h at 4 °C. After washing, the membranes were incubated with Palivizumab (200 μg/mL; Synagis®, Abbvie, Wavre, Belgium) during 1 h at room temperature. The membranes were washed and incubated with horseradish peroxidase-conjugated goat secondary anti-human IgG (KPL, Gaithersberg, MD, USA) for 45 min at room temperature. Bound virus were revealed by 1-step ultra TMB-blotting solution (Pierce).

2.12. Molecular docking

Three-dimensional structures of BPI (Bactericidal Permeability Increasing Protein; PDB 1EWF), motavizumab antibody (PDB ID 3IXT), and pre-fusion (PDB ID 4JHW) and post-fusion (PDB ID 3RRR) F protein were obtained from the Protein Data Bank database. The molecular docking procedures were performed by the online platform PatchDock® (Duhovny et al., 2002), and the generated data were refined by the online FireDock® server (Mashiach et al., 2008). The parameters for the docking were kept standard, with a value of root-mean-square deviation (RMSD) = 4. The complexes and data were analyzed using Chimera® graphic interface software, which was also used to generate images.

3. Results and discussion

3.1. Generation of NETs by PMA-stimulated neutrophils

The process of Netose activated by PMA and hRSV are similar. Both stimuli induce suicidal Netose in a ROS-dependent manner and these NETs present DNA, elastase and myeloperoxidase in their composition (Funchal et al., 2015). Thus, PMA stimulus was used to obtain NETs in large quantities. NETs generated by PMA stimulation (50 nM for 3 h) were evaluated morphologically by fluorescence microscopy and electrophoretically using agarose and polyacrylamide gels. Unstimulated neutrophils did not release NETs, whereas PMA-stimulated neutrophils produced extracellular structures that were stained by DAPI, a fluorescent DNA intercalator (Fig. 1a,b). DNA present in NETs is decondensed, intact, and predominantly negatively charged, and can trap pathogens and prevent their dissemination (Halverson et al., 2015). Analysis of the DNA electrophoretic profile, using agarose gels, revealed the presence of long and homogeneous DNA fragments greater than 10,000 base pairs (Fig. 1c). Proteins described as components of NETs include histones, elastase, and myeloperoxidase, among others (Najmeh et al., 2015). The protein content of NETs generated in this study was analyzed using 12% and 20% polyacrylamide gels (Fig. 1d,e). Silver nitrate staining of 12% gels resulted in the presence of three proteins with molecular weights of approximately 75, 50, and 30 kDa. Based on the protein composition of NETs and the determined molecular weights, we suggest that these bands correspond to elastase (28.5 kDa), cathepsin G (28.8 kDa), and myeloperoxidase (73.8–87.2 kDa) (Fig. 1d). Increasing the gel acrylamide concentration resulted in the appearance of additional bands with a molecular weight of approximately 15 kDa; it was suggested that these proteins might be histones (11–15 kDa) (Fig. 1e). Therefore, in our hands, the structures released by PMA-stimulated neutrophils exhibited comparable morphology and content (DNA and proteins) to those previously described in the literature. These observations were of paramount importance for the subsequent experiments.

3.2. NETs heated to 40 °C maintain their activity relative to human physiological temperature

After the collection of the NET-rich supernatant, it was possible to observe large clusters of whitish material, similar to cotton, that were visually identified as DNA. For this material to be dissolved without the use of DNAase, samples were maintained for 24 h in a water bath at 40 °C. This was important as the use of DNAse would result in excessive fragmentation of DNA, which could interfere with viral capture by NETs (Barrientos et al., 2013). The enzymatic activity of myeloperoxidase was monitored to evaluate whether heating the samples to 40 °C would impair the biological function of NETs. Fresh NETs were assumed to have 100% myeloperoxidase enzymatic activity (Fig. 2). Incubation of NETs in a water bath for 24 h at 37 or 40 °C resulted in decreases in enzymatic activity of 43.76% and 45.36%, respectively. In terms of enzymatic activity, there was no statistically significant

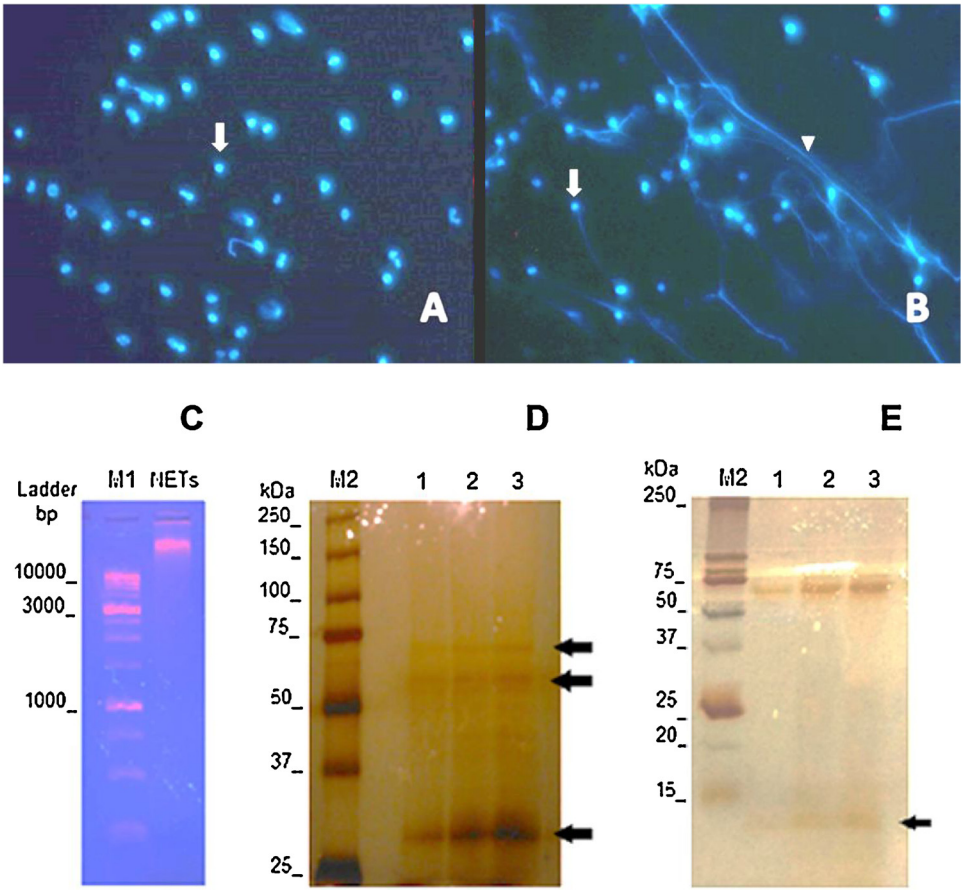


Fig. 1. Neutrophil extracellular traps (NETs) induced by phorbol myristate acetate (PMA) stimulation. Neutrophils (2×10^5) (white arrow) were incubated with only FBS-free DMEM-F12 (a) or in the presence of 50 nM PMA (b). Images of the NETs (white arrowhead) are representative of two independent assays performed in triplicate. (c) Electrophoretic analysis of NETs in 1.5% agarose gel, where M1 = molecular DNA marker (1 kb DNA ladder). Electrophoretic analysis of NETs on 12% (D) and 20% (E) polyacrylamide gels after staining with silver nitrate. M2 = molecular weight marker (10–250 kDa), 1–3 = NETs 12.5–50 μg/ml); black arrows = major bands. The images are representatives of three experiments.

difference between NETs heated to 37 and 40 °C. This result had biological relevance based on the human physiological temperature of 37 °C. Among the main components of NETs, histones begin to exhibit structural changes at approximately 65 °C; specifically, elastase undergoes denaturation at 59 °C (Weischet et al., 1978; Byler et al., 1999), whereas myeloperoxidase is structurally stable at temperatures up 80 °C (Banerjee et al., 2011). According to Wallace et al. (1979), DNA has a melting temperature (the temperature at which half of the sequence is denatured) of 76.2 °C, and begins to undergo denaturation at approximately 70 °C (Wang et al., 2014). These data demonstrate that heating the sample to 40 °C has no detrimental biological effect on NETs, and therefore this treatment was suggested to not affect the results presented herein.

3.3. Cellular cytotoxicity of NETs on HEp-2 cells

Before assessing the effects of NETs on hRSV infection of HEp-2 cells, it was necessary to investigate any cytotoxic effects. Different concentrations of NETs (0.06– 67 μg/ml) were incubated with HEp-2 cells (5×10^4) and viability was evaluated after 4 d in culture in FBS-free DMEM-F12 medium (Fig. 3). Cells not treated with NETs were assumed to be 100% viable. NETs demonstrated a dose-dependent

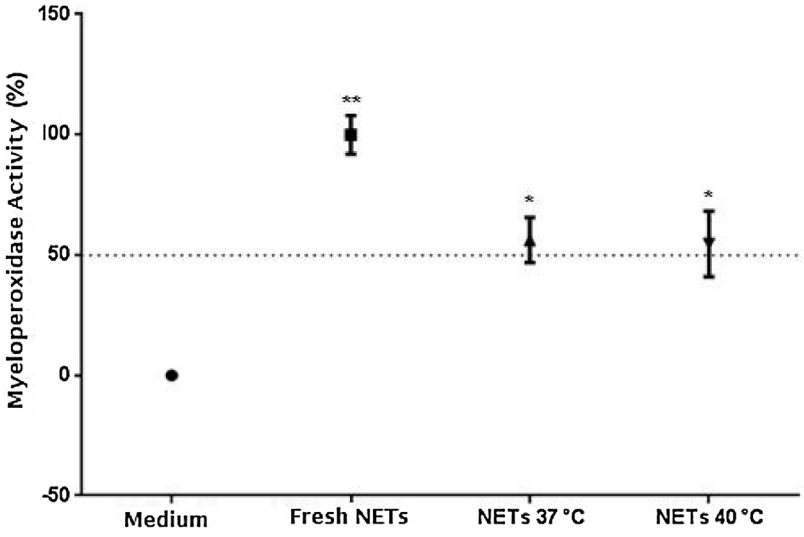


Fig. 2. Evaluation of myeloperoxidase activity. Neutrophil extracellular traps (NETs) that passed the water bath stage at 37 °C and 40 °C, as well as fresh NETs (without heating) were incubated with myeloperoxidase substrate for 1 h. Absorbance readings were taken at 405 nm. Culture medium (DMEM F12) was used as a negative control and fresh NETs were assumed used as the positive control (100% activity). The graph is representative of three independent experiments performed in triplicate. The result represents the mean values obtained ± standard deviation (*$p < 0.05$, **$p < 0.01$).

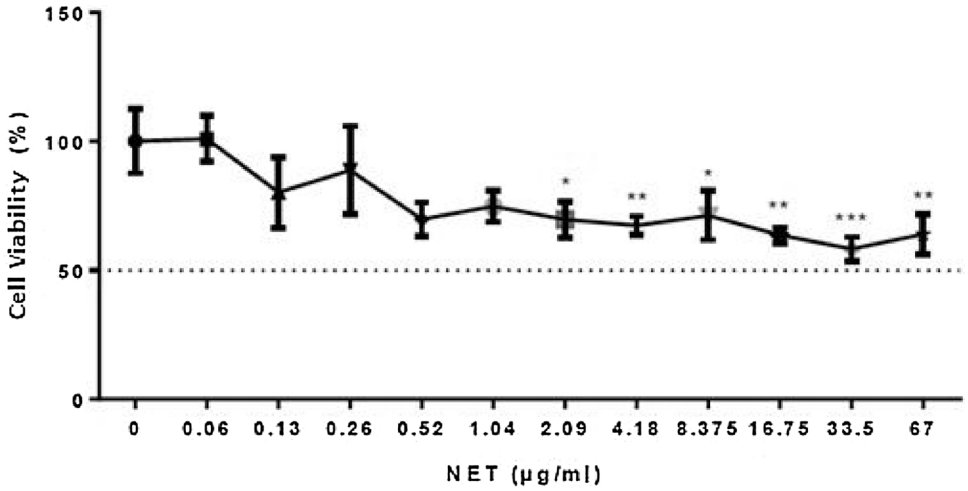


Fig. 3. Determination of CC_{50} of neutrophil extracellular traps (NETs) on HEp-2 cells. HEp-2 (5×10^4) cells were cultured in the presence of different concentrations of NETs (0–67 µg/ml) for 4 d at 37 °C. Cell viability was assessed by performing MTT assays. The absorbance reading was measured at 560 nm and converted into the percent viable cells, assuming the cell control (NETs = 0 µg/ml) to be 100% viable. The graph is representative of three independent experiments performed in triplicate. The curve shows the results of the mean values obtained ± standard deviation (*p < 0.05, **p < 0.01, ***p < 0.001).

cytotoxic effect, as demonstrated by Saffarzadeh et al. (2012), and resulted in statistically significant cell death (up to 32% compared to viability of the control) at concentrations ≥ 2 µg/ml. None of the tested concentrations resulted in cell death exceeding 50%, even at the highest concentration of 67 µg/ml. Saffarzadeh et al. (2012) analyzed the influence of NETs (3–10 µg/ml for 16 h) on epithelial (MLE-12 and AT-II) and endothelial (A549, HPAEC, and HUVEC) cells and found that histones are primarily responsible for cell damage induced by NETs. No studies had previously been conducted assessing the cytotoxicity of NETs on Hep-2 cells. Previous data have shown that compared to A549 cells Hep-2 cells can be more or less sensitive to cell death depending on the stimulus (Chang, 2013; Rooney and Ryan, 2005). Our results suggest that Hep-2 cells are less sensitive to cell death induced by NETs than A549 cells. In addition, we demonstrated that NETs have a CC_{50} > 67 µg/ml for Hep-2 cells.

3.4. NETs exhibit anti-hRSV action

Antiviral agents can have an inhibitory effect on infection due to direct or indirect effects on cells and/or viral particles. Studies have demonstrated the ability of NETs to inhibit infection by sequestering or neutralizing viral particles (Jenne and Kubes, 2015). Through their DNA network, NETs can capture viral particles, preventing them from reaching the target cell, or neutralize viral particles through the action of their proteins such as myeloperoxidase, defensins, and histones (Collins et al., 2001; Funchal et al., 2015; Hoeksema et al., 2015). After the cytotoxic evaluation of NETs using HEp-2 cells, their effect on *in vitro* infection by hRSV was assessed. Before infection, different concentrations of viral particles (MOIs of 0.1, 0.5, and 1) were incubated with different concentrations of NETs (0.5–64 µg/ml) for 1 h at 4 °C. After 4 d of culture, cell viability was determined by performing MTT assays (Fig. 4). Cell morphology and syncytium formation were also analyzed microscopically after 3 d of culture for all treatments (Fig. 5).

Incubation of an MOI 0.1 viral inoculum with NETs resulted in cell protection greater than 50% at concentrations < 16 µg/ml, with more effective and statistically significant protection observed at concentrations ranging from 2 to 8 µg/ml. Cell protection decreased with increasing concentrations of NETs (> 32 µg/ml), which resulted in increased cell damage and decreased viability (Fig. 4a). In addition, at concentrations > 2 µg/ml, there was a reduction in syncytium count of greater than 50% (Fig. 4b). Increased concentrations of NETs (≥ 32 µg/ml) strongly reduced the number of syncytia, whereas cell damage was also observed (Fig. 4a,b). NETs at a concentration of 64 µg/ml resulted in intense cellular damage, greater than that caused by viral infection (viral control). Based on morphological analysis (Fig. 5), viral control cells exhibited elongated morphology, a reduction in the number of cells, and a high number of syncytia. Low concentrations of NETs (1 µg/ml) resulted in high syncytia counts. However, these were associated with a reduction in size and are therefore difficult to visualize in the presented images. For concentrations of NETs that protected cells from cellular damage (< 8 µg/ml), there was a marked decrease in the number of syncytia, relative to that observed for the viral control; in addition, the syncytia in these conditions were smaller. With higher concentrations of NETs (≥ 16 µg/ml) there was an increasing absence of adherent cells and a decrease in the formation of syncytia, which were observed to be larger than those observed with other conditions.

The viral inoculum (MOI) was increased to enhance the protective effect of NETs. When using a five-fold larger inoculum (MOI = 0.5), we obtained results similar to those using an MOI of 0.1 (Fig. 4). NETs (1–8 µg/ml) maintained a minimum cell protective effect of 50%, and were associated with a decrease in the number of syncytia (Fig. 4c,d). Concentrations ≥ 16 µg/ml were not considered effective; whereas these treatments reduced the number of syncytia, adverse effects were observed regarding the number of viable cells and the size of the syncytia (Fig. 5).

Increasing the viral inoculum to a MOI of 1 (10-fold higher) resulted in a marked reduction in the anti-hRSV effects of NETs. None of the NET concentrations tested could prevent or reverse cellular damage caused by viral infection, resulting in no statistically significant protection (Fig. 4e). The lack of cellular protection at this concentration might indicate a limited inhibitory effect of NETs with a high viral load. Although cell protection was not observed based on viability assay, the number of syncytia were significantly reduced relative to that of the viral control, and concentrations of 2 and 4 µg/ml were most effective (Fig. 4f). However, based on morphological analysis of cells (Fig. 5), all concentrations resulted in a marked reduction in the number of cells that adhered to the well, the presence of elongated cells, and a high number of syncytia. At the highest NET concentration (64 µg/mL), we observed a reduced cell number into well. The few remaining cells undergo fusion and show large syncytia. The simultaneous presence of virus and NETs during cell culture appeared to aggravate the individual cytotoxic effects of each, resulting in a smaller number of cells and consequently a smaller number of syncytia, but with increased dimensions.

The data obtained demonstrate the anti-hRSV action of NETs (2–8 µg/ml), with a direct effect on viral particles, suggesting that there is a physical interaction between the virus and the DNA/protein structure. During hRSV replication, the formation of syncytia is related to the tissue dispersion of the virus. The reduction in the number and size of syncytia with NET treatment (2–4 µg/ml) could indicate that NETs are interfering with the cellular fusion protein (F). The virucidal effect of NETs was strongly dependent on viral load. Cortjens et al.

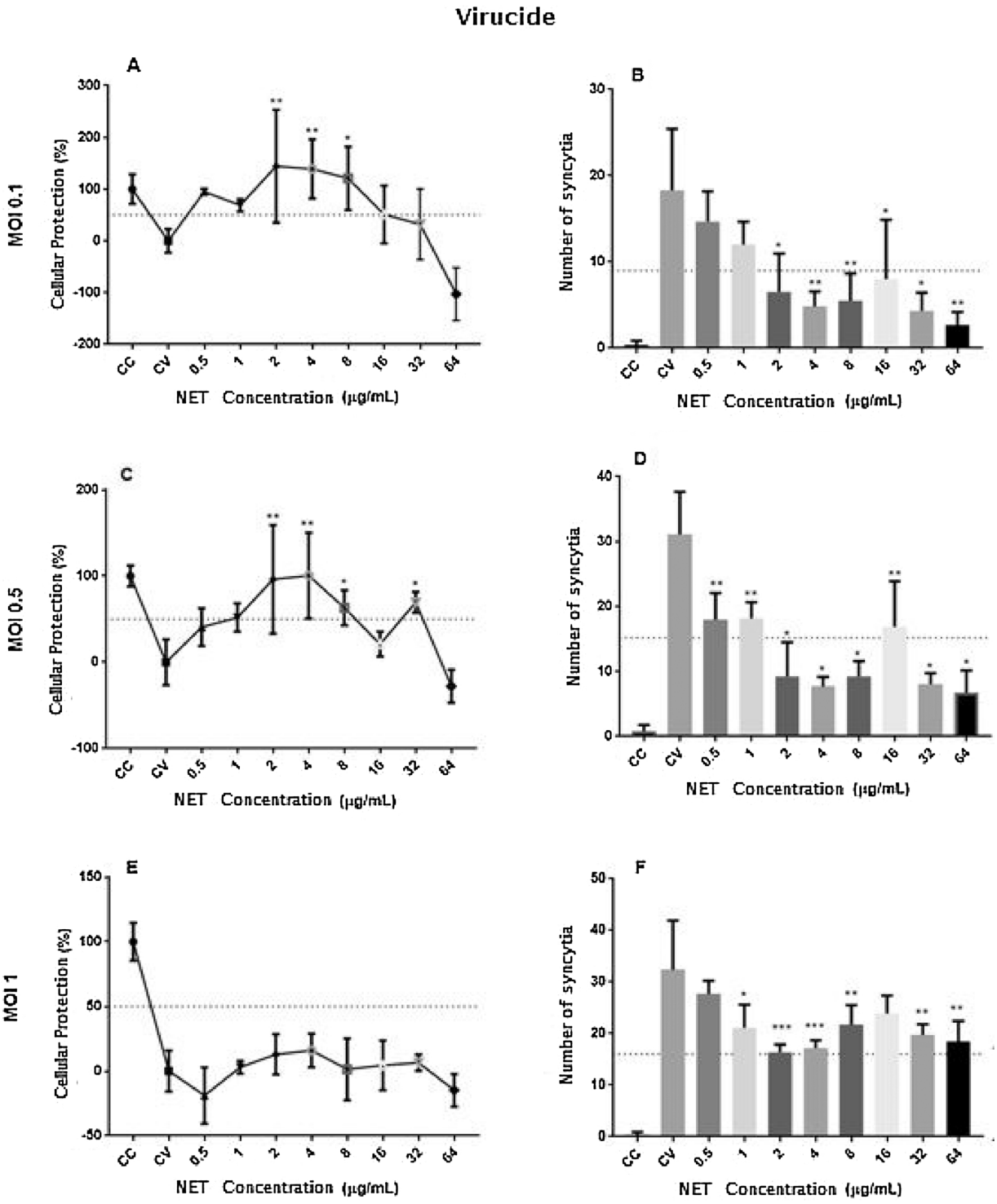


Fig. 4. Determination of CE_{50} of neutrophil extracellular traps (NETs) on human respiratory syncytial virus (hRSV). Virucidal effect of NETs (0.5–64 µg/ml) on hRSV (MOI = 0.1, 0.5, and 1) based on the evaluation of % cellular protection (a, c, e) and quantification of syncytia formation (b, d, f). The graph is representative of three independent experiments performed in triplicate. The curve shows the results of the mean values obtained ± standard deviation (*p < 0.05, **p < 0.01, ***p < 0.001).

(2016) demonstrated that hRSV viral particles (MOI, 0.03–0.4), in the presence of activated neutrophils, are captured by NETs, preventing viral infection of cells. The observed benefits of NETs should be analyzed with caution since an intense neutrophil response might contribute to the pathology of this viral infection. During our analyses, the presence of NETs (> 16 µg/ml), even at lower concentrations than the CC_{50} value (67 µg/ml), resulted in increased cell damage in the presence of virus. The presence of NETs in the lung tissue of individuals infected with hRSV has been identified as one of the immunopathological mechanisms involved in airway obstruction and tissue damage. These mechanisms decrease the ventilation capacity of the individual, the reaction to treatment, and the quality of life (Brinkmann et al., 2010; Najmeh et al., 2015). Studies on antiviral compounds use the selectivity index ($SI = CC_{50}/CE_{50}$) to relate

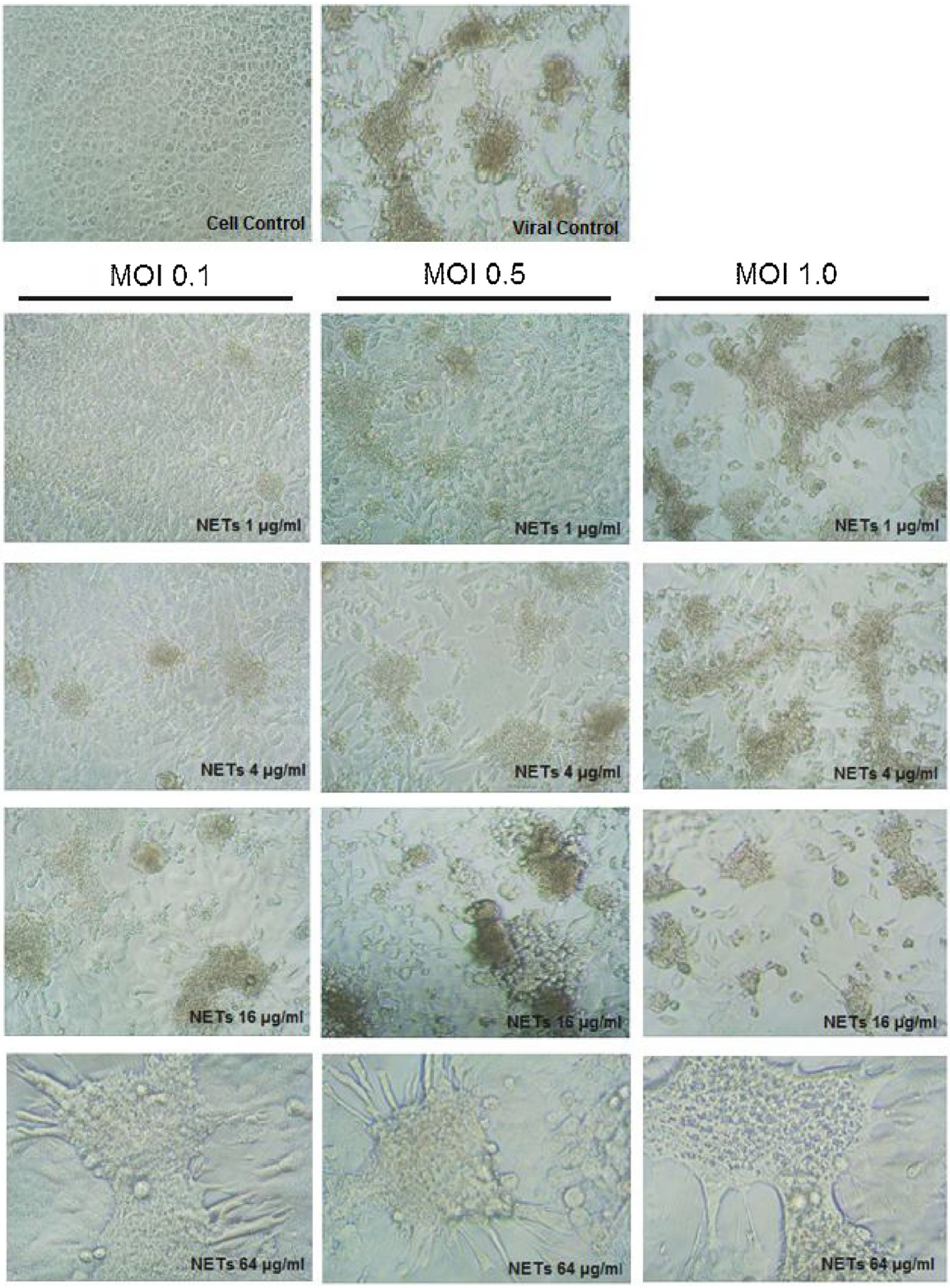


Fig. 5. Morphology of human respiratory syncytial virus (hRSV)-infected HEp-2 cells (MOI = 0.1, 0.5, and 1.0) after treatment with different concentrations of neutrophil extracellular traps (NETs) (0.5–64 µg/ml). Uninfected cells were used as the cell control. Infected cells were designated as the viral control. The images were evaluated and documented using a white light microscope (40×).

cytotoxicity (CC_{50}) to effectiveness (CE_{50}) of a given molecule. Compounds with promising antiviral action are characterized by SI values ≥4 (Sidwell, 1986). The CC_{50} (> 67 µg/ml) and CE_{50} values (~1 µg/ml) for NETs, using viral MOIs of 0.1 and 0.5, correspond to an SI value of ~67. Under these conditions, we speculate that the presence of NETs would be beneficial for the elimination of viral particles. In contrast, an increase in viral load (MOI 1.0) appears to reduce this effect.

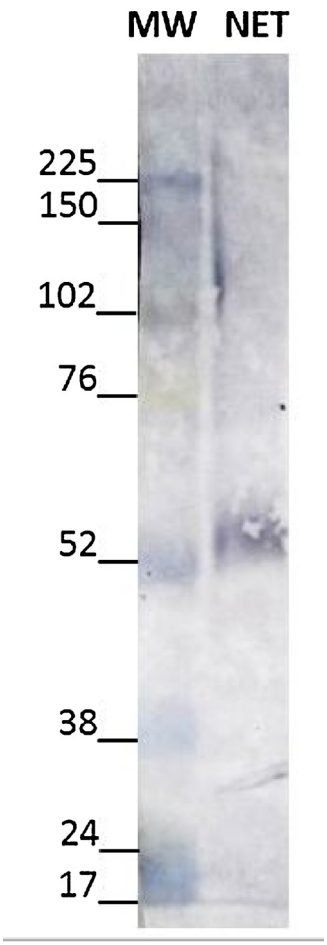


Fig. 6. Interaction between NET protein components and the hRSV. NET protein components, immobilized in a nitrocellulose membrane, were incubated with hRSV solution. Bound virus were revealed using antibodies (Palivizumab and horseradish peroxidase-conjugated goat secondary anti-human IgG) and ultra TMB-blotting solution.

3.5. Components of NETs interact with RSV

Western blotting assay was performed to evaluate the possible interaction between NET protein components and the hRSV. The results indicated that hRSV interacts with a protein from NETs (Fig. 6) This protein has an apparent 52–60 kDa molecular weight. Among protein components described for NETs, BPI (bactericidal permeability increasing protein) is a monomer with 55 kDa molecular size. Some works have described a role of BPI during viral infections. BPI negatively regulates coxsackievirus B (CVB) replication (Morosky et al., 2016; Delorme-Axford et al., 2014) and inhibits the infectivity of Influenza A virus (Pinkenburg et al., 2016).

In order, molecular docking was used to complement the investigation and interpret the *in vitro* experimental data and better to evaluate the interaction between BPI protein and the hRSV F protein. The F protein was used in both conformation states, both pre- and post-fusion, since both are present on the surface of the viral particle, and comprise approximately 50% of the viral surface (Liljeroos et al., 2013). The F protein of hRSV is critical for viral infection (McLellan et al., 2013), and has recently been described to stimulate the release of NETs (Funchal et al., 2015). Among NET component molecules, DNA has high potential for pathogen capture due to its size and physicochemical characteristics. Such effects are increased and enhanced by the presence of various microbicidal proteins, such as BPI (Dąbrowska et al., 2016).

The structure of the motavizumab antibody (PDB ID 3IXT), known to interact with the F protein, was obtained for comparison purposes.

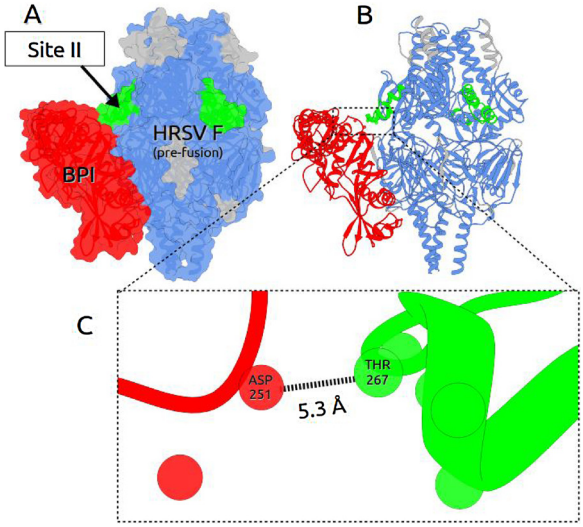


Fig. 7. Model of the interaction between the pre-fusion F protein and BPI, generated by the PatchDock server. (a) Surface model, in which it is possible to see the first predicted complex formed by the two proteins. (b) The regions of interaction (green) occur at site II of the F protein. (c) The lowest distance between the pre-fusion F protein site II closest residue to BPI interaction regions, as measured by the Chimera viewer (For interpretation of the references to colour in this figure legend, the reader is referred to the web version of this article).

Molecular docking between motavizumab and the F protein trimer resulted in interactions with the antibody at the A site of the F protein in both conformations, as described in the literature (McLellan et al., 2011) (Supplementary Fig. 1). The motavizumab antibody interacts with the A site (site II) of the F protein, which neutralizes virus fusion with the cell (McLellan et al., 2010). The energy associated with these interactions was found to be −11.31 kcal/mol and −29.4 kcal/mol, for the pre-fusion and post-fusion conformations, respectively. The generated model resulted in high scores for both pre-fusion and post-fusion forms (14,170 and 15372, respectively).

The molecular docking between F protein in pre-fusion state and BPI resulted in three possible complex. The energy obtained (−22.05; −19.70; −12.01 kcal/mol) demonstrate high stability of the complex, compared to F-protein-motavizumab complex. Associated scores (18858, 17,932 and 17,172) were also higher, indicating a high probability that the formed complexes are viable. The complexes were different when we analyze the interaction sites. In the first complex, BPI interacts very close to site II (motavizumab site of interaction) with average distance of 6.6 Å (Fig.7). This site is related to inhibition of viral particles (McLellan et al., 2010). The others complex occurred near to site IV (antibody 101 F site of interaction) (McLellan et al., 2010) and to site I. These sites generate poor viral neutralization activity on pre-fusion F protein (Killikelly et al., 2016) but they can help in the capture viral role. The complex generated might result in inhibition of viral particle fusion activity, thus contributing to the antiviral action of NETs.

The only predicted complex between F protein in post-fusion state and BPI (Fig.8) demonstrated binding energy of −5.66 kcal/mol, that is lower than F protein in pre-fusion state, but still viable to form complexes and the associated score was 16,970. The interaction region is located very close to site IV (antibody 101 F site of interaction) with average distance of 6.3 Å, indicating inhibition of viral particle fusion activity (McLellan et al., 2010). Neutralization of F protein at site II (pre-fusion) and IV (post-fusion) can lead to inhibition of viral fusion activity with the host cell, whereas neutralization of the F protein at site I can lead to inactivation of cell-cell fusion in infected cells.

The presence of NETs in the airway results in a delicate balance between beneficial and detrimental effect during the ongoing infectious

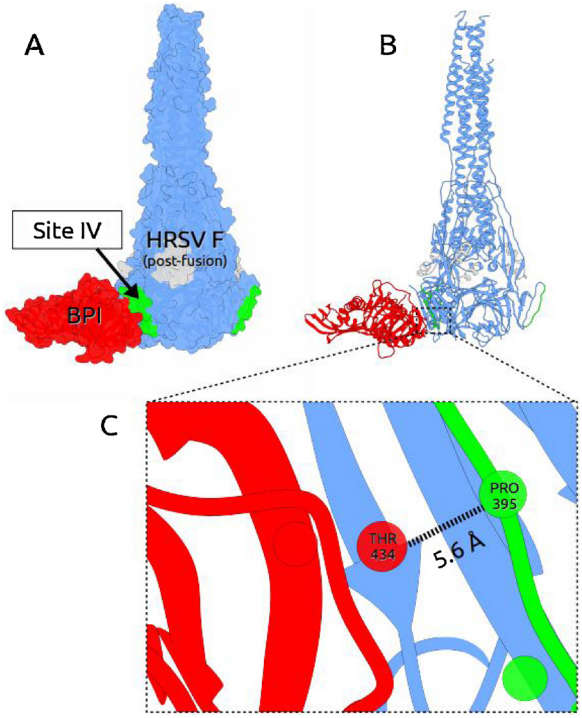


Fig. 8. Model of the interaction between the post-fusion F protein and BPI, generated by the PatchDock server. (a) Surface model, in which it is possible to see the only complex formed by the two proteins. (b) The regions of interaction (green) occur at site IV of the F protein. (c) The lowest distance between the post-fusion F protein site IV closest residue to BPI interaction regions, as measured by the Chimera viewer. (For interpretation of the references to colour in this figure legend, the reader is referred to the web version of this article).

process. Elevated concentrations of NETs result in tissue damage, whereas lower levels might promote the capture and inhibition of hRSV, through interactions between the viral F protein and NET proteins (BPI). These interactions could block viral F protein functions, thereby affecting early virus cycle steps such as adhesion and internalization, as well as viral spread, by inhibiting cell-cell fusion, and consequently syncytium formation.

4. Conclusion

We demonstrated *in vitro* that low concentrations of NETs exhibit promising anti-hRSV activity, based on their virucidal effect, high selectivity index (SI = 67), and effect on reducing virus-mediated cell damage and syncytium formation. *In silico* interactions between the virus F protein and NET proteins, specifically, BPI, might be at least partially responsible for such effects by promoting virus neutralization. However, our recent studies and others suggest that the airways of individuals infected with hRSV are obstructed by a large number of NETs, which are stimulated by the virus itself, and could contribute to the immunopathology observed in children infected with this virus (Cortjens et al., 2016; Funchal et al., 2015). In addition to broadening the understanding of the role of NETs during viral infection, as well as their relationship with hRSV, these results demonstrate the need for experimental and clinical approaches to modulate the detrimental effects of NETs during pulmonary disease. Future studies might contribute to the development of new treatments and strategies to combat hRSV, helping to reduce infections and control the disease, especially in immunocompromised individuals.

Ethics statement

The experimental procedures using human blood were approved by the Local Ethics Committee in Human Research of the Faculdade de Ciências e Letras de Assis – FCL UNESP (42,048,315.5.0000.540). Written informed consent, suggested and approved by the Committee, was obtained from each participant before beginning the investigation procedures.

Conflicts of interest

None.

Funding

The authors are grateful for the financial support from CAPES (master's scholarship) and FAPESP (Grant 2016/03867-3).

Acknowledgement

We thank PhD Marcelo Fábio G. Nogueira for his help efforts with microscopics analysis.

Appendix A. Supplementary data

Supplementary material related to this article can be found, in the online version, at doi:https://doi.org/10.1016/j.virusres.2018.04.001.

References

Banerjee, S., Stampler, J., Furtmüller, P.G., Obinger, C., 2011. Conformational and thermal stability of mature dimeric human myeloperoxidase and a recombinant monomeric form from CHO cells. Biochim. et Biophys. 1814, 375–387.

Barrientos, L., Marin-Esteban, V., de Chaisemartin, L., Le Moal, V.L., Sandré, C., Bianchini, E., 2013. An improved strategy to recover large fragments of functional human neutrophil extracellular traps. Front. Immunol. 4, 166.

Brinkmann, V., Laube, B., Abu Abed, U., Goosmann, C., Zychlinsky, A., 2010. Neutrophil extracellular traps: how to generate and visualize them. J. Vis. Exp. 24, e1724.

Brinkmann, V., Reichard, U., Goosmann, C., Fauler, B., Uhlemann, Y., Weiss, D.S., et al., 2004. Neutrophil extracellular traps kill bacteria. Science 303, 1532–1535.

Byler, D.M., Lee, D.L., Randall, C.S., 1999. Thermal denaturation of elastase in the presence and absence of guanidinium chloride: an IR spectroscopic and DSC investigation. ACS Symposium Series 7. pp. 145–158.

Chang, J.S., 2013. Fresh ginger (*Zingiber officinale*) has anti-viral activity against human respiratory syncytial virus in human respiratory tract cell lines. J. Ethnopharmacol. 145, 146–151.

Chevallet, M., Luche, S., Rabilloud, T., 2006. Silver staining of proteins in polyacrylamide gels. Nat. Protoc. 1, 1852–1858.

Collins, P.L., Chanock, R.M., Amurphy, B.R., 2001. Respiratory syncytial virus. In: Knipe, D.W., Howley, P.M. (Eds.), Fields Virology, 4th edition. Wolter Kluwer, Philadelphia, Pennsylvania, USA, pp. 1443–1486.

Cortjens, B., De Boer, O.J., De Jong, R., Antonis, A.F.G., Sabogal Piñeros, Y.S., Lutter, R., et al., 2016. Neutrophil extracellular traps cause airway obstruction during respiratory syncytial virus disease. J. Pathol. 238, 401–411.

Dąbrowska, D., Jabłońska, E., Garley, M., Ratajczak-Wrona, W., Iwaniuk, A., 2016. New aspects of the biology of neutrophil extracellular traps. Scand. J. Immunol. 84, 317–322.

Delorme-Axforda, E., Moroskya, S., Bombergera, J., Stolzb, D.B., Jacksonc, W.T., Coynea, C.B., 2014. BPIFB3 regulates autophagy and coxsackievirus B replication through a noncanonical pathway independent of the core initiation machinery. mBio 5 e02147-14.

Duhovny, D., Nussinov, R., Wolfson, H.J., 2002. Efficient unbound docking of rigid molecules, Gusfield et al.,, Proceedings of the 2'nd Workshop on Algorithms in Bioinformatics(WABI) Rome, Italy, Lecture Notes in Computer Science, Springer Verlag, pp. 185–200.

Funchal, G.A., Jaeger, N., Czepielewski, R.S., Machado, M.S., Muraro, S.P., Stein, R.T., et al., 2015. Respiratory syncytial virus fusion protein promotes TLR-4-dependent neutrophil extracellular trap formation by human neutrophils. PLoS One 10, e0124082.

Green, M.R., Sambrook, J., 2012. Molecular Cloning. A Laboratory Manual, 4th ed. Cold Spring Harbor Laboratory Press.

Gupta, C.K., Leszczynski, J., Gupta, R.K., Siber, G.R., 1996. Stabilization of respiratory syncytial virus (RSV) against thermal inactivation and freeze-thaw cycles for development and control of RSV vaccines and immune globulin. Vaccine 14, 1417–1420.

Hall, C.B., Walsh, E.E., Long, C.E., Schnabel, K.C., 1991. Immunity to and frequency of reinfection with respiratory syncytial virus. J. Infect. Dis. 163, 693–698.

Halverson, T.W.R., Wilton, M., Poon, K.K.H., Petri, B., Lewenza, S., 2015. DNA Is an antimicrobial component of neutrophil extracellular traps. PLoS Pathog. 11, e1004593.

Hoeksema, M., Tripathi, S., White, M., Qi, L., Taubenberger, J., Van Eijk, M., et al., 2015.

Arginine-rich histones have strong antiviral activity for influenza A viruses. Innate Immun. 21, 736–745.
Huang, K., Incognito, L., Cheng, X., Ulbrandt, N.D., Wu, W., 2010. Respiratory syncytial vrus-neutralizing monoclonal antibodies motavizumab and palivizumab inhibit fusion. J. Virol. 84, 8132–8140.
Jenne, C.N., Kubes, P., 2015. Virus-induced NETs – critical component of host defense or pathogenic mediator? PLoS Pathog. 11, e1004546.
Jenne, C.N., Wong, C.H., Zemp, F.J., McDonald, B., Rahman, M.M., Forsyth, P.A., et al., 2013. Neutrophils recruited to sites of infection protect from virus challenge by releasing neutrophil extracellular traps. Cell. Host Microbe 13, 169–180.
Killikelly, A.M., Kanekiyo, M., Graham, B.S., 2016. Pre-fusion F is absent on the surface of formalin-inactivated respiratory syncytial virus. Sci. Rep. 6, 34108.
Liljeroos, L., Krzyzaniakb, M.A., Heleniusb, A., Butchera, S.J., 2013. Architecture of respiratory syncytial virus revealed by electron cryotomography. Proc. Natl. Acad. Sci. U.S.A. 27, 11133–11138.
Mashiach, E., Schneidman-Duhovny, D., Andrusier, N., Nussinov, R., Wolfson, H.J., 2008. FireDock: a web server for fast interaction refinement in molecular docking. Nucleic Acids Res. 36, W229–232.
McKimm-Breschkin, J.L., 2004. A simplified plaque assay for respiratory syncytial virus—direct visualization of plaques without immunostaining. J. Virol. Methods 120, 113–117.
McLellan, J.S., Chen, M., Joyce, M.G., Sastry, M., Stewart-Jones, G.B., Yang, Y., et al., 2013. Structure-based design of a fusion glycoprotein vaccine for respiratory syncytial virus. Science 342, 592–598.
McLellan, J.S., Chen, M., Kim, A., Yang, Y., Graham, B.S., Kwong, P.D., 2010. Structural basis of respiratory syncytial virus neutralization by motavizumab. Nat. Struct. Mol. Biol. 17, 248–250.
McLellan, J.S., Yang, Y., Graham, B.S., Kwong, P.D., 2011. Structure of respiratory syncytial virus fusion glycoprotein in the postfusion conformation reveals preservation of neutralizing epitopes. J. Virol. 85, 7788–7796.
Morosky, S., Lennemann, N.J., Coyne, C.B., 2016. BPIFB6 regulates secretory pathway trafficking and enterovirus replication. J. Virol. 90, 5098–5107.
Najmeh, S., Cools-Lartigue, J., Giannias, B., Spicer, J., Ferri, L.E., 2015. Simplified human neutrophil extracellular traps (NETs) isolation and handling. J. Vis. Exp. 16, e52687.
Petricevich, V.L., Mendonca, R.Z., 2003. Inhibitory potential of *Crotalus durissus terrificus* venom on measles virus growth. Toxicon 42, 143–153.
Pinkenburg, O., Meyer, T., Bannert, N., Norley, S., Bolte, K., Czudai-Matwich, V., Herold, S., Gessner, A., Schnare, M., 2016. The human antimicrobial protein Bactericidal/Permeability-Increasing protein (BPI) inhibits the infectivity of influenza A virus. PLoS One 11, e0156929.
Porto, B.N., Stein, R.T., 2016. Neutrophil extracellular traps in pulmonary diseases: too much of a good thing? Front. Immunol. 7, 311.
Rasmussen, L., Maddox, C., Moore, B.P., Severson, W., White, E.L., 2011. A high-throughput screening strategy to overcome virus instability. Assay Drug Dev. Technol. 9, 184–190.
Rooney, S., Ryan, M.F., 2005. Effects of alpha-hederin and thymoquinone, constituents of *Nigella sativa*, on human cancer cell lines. Anticancer Res. 25, 2199–2204.
Rzepka, J.P., Haick, A.K., Miura, T.A., 2012. Virus-infected alveolar epithelial cells direct neutrophil chemotaxis and inhibit their apoptosis. Am. J. Respir. Cell. Mol. Biol. 46, 833–841.
Saffarzadeh, M., Juenemann, C., Queisser, M.A., Lochnit, G., Barreto, G., Galuska, S.P., et al., 2012. Neutrophil extracellular traps directly induce epithelial and endothelial cell death: a predominant role of histones. PLoS One 7, e32366.
Saitoh, T., Komano, J., Saitoh, Y., Misawa, T., Takahama, M., Kozaki, T., et al., 2012. Neutrophil extracellular traps mediate a host defense response to human immunodeficiency virus-1. Cell. Host Microbe 12, 109–116.
Sidwell, R.W., 1986. Overview of viral agents in pediatric enteric infections. Pediatr. Infect. Dis. 5, S44–S45.
Sousa-Rocha, D., Thomaz-Tobias, M., Diniz, L.F.A., Souza, P.S.S., Pinge-Filho, P., Toledo, K.A., 2015. *Trypanosoma cruzi* and its soluble antigens induce NET release by stimulating toll-like receptors. PLoS One 10, e0139569.
Von Köckritz-Blickwede, M., Chow, A.O., Nizet, V., 2009. Fetal calf serum contains heat-stable nucleases that degrade neutrophil extracellular traps. Blood 114, 5245–5246.
Wallace, R.B., Shaffer, J., Murphy, R.F., Bonner, J., Hirose, T., Itakura, K., 1979. Hybridization of synthetic oligodeoxyribonucleotides to phi chi 174 DNA: the effect of single base pair mismatch. Nucleic Acids Res. 6, 3543–3557.
Wang, X., Lim, H.J., Son, A., 2014. Characterization of denaturation and renaturation of DNA for DNA hybridization. Environ. Health Toxicol. 29, e2014007.
Weischet, W.O., Tatchell, K., Van Holde, K.E., Klump, H., 1978. Thermal denaturation of nucleosomal core particles. Nucleic Acids Res. 5, 139–160.